ON-LINE APPENDIX

Voxel-Based Morphometric Analysis

Imaging Protocol. T1-weighted structural MR images were obtained with the following parameters: TR = 25 ms, TE = 4.6 ms, section thickness = 1.2 mm, no section gap, section number = 140, flip angle = 30°, and in-plane resolution = 256 × 256 (0.94 × 0.94 mm). For each subject, 1 T1-weighted structural image was obtained on an Intera 1.5T MR scanner (Philips Healthcare) during a single image session.

Data Preprocessing. Data preprocessing was performed by using SPM8. First, the new-segment procedure was used to segment the MR images into 6 partitions, including GM, WM, CSF, and 3 other background partitions based on a modified mixed-model cluster analysis technique. The new segment procedure is generally more robust than using the "segment" button. Next, GM and WM templates were generated from the entire image dataset by using the Diffeomorphic Anatomical Registration Through Exponentiated Lie Algebra Toolbox (SPM8) technique, which matches the GM and WM to each other.[1] Finally, GM and WM images were spatially normalized to the GM and WM templates that were created in the second step and then were smoothed by an isotropic Gaussian filter with a 6-mm full width at half maximum kernel. The GM and WM concentration maps were obtained.

Statistical Analysis. The GM and WM concentration maps of the patients and controls were used for statistical analysis. The patients and healthy subjects were compared by using the "Specify 2nd-level" routine in SPM8. Two-sample *t* tests were applied to make group comparisons of the patients and healthy controls. The findings in On-line Fig 2 were considered significant at a voxel level of $P < .001$, uncorrected for multiple comparisons.

On-line Fig 2*A* shows the GM comparison between the patients and the controls, while On-line Fig 2*B* is the WM comparison.

The most significant difference in GM between the 2 groups of subjects is that the concentration in the right temporal lobe is reduced and the concentration in the left temporal lobe is increased in patients compared with healthy controls. The second difference is that the concentration decreased more in the right hemisphere than in the left hemisphere, while the concentration increased more in the left hemisphere than in the right hemisphere. The left and the right sides of the cerebellum present a similar phenomenon. Overall, the decreased GM concentration is more prevalent than the increased GM concentration in the patients with R-mTLE.

The WM concentration in the right temporal lobe and subcortex significantly decreased; however, the WM concentration in the left temporal lobe and subcortex slightly decreased. The WM concentration in most parts of the cerebral cortex increased (the WM concentration in the sensorimotor cortex and dorsal temporal cortex decreased). Overall, the WM concentration in the left hemisphere increased more than that in the right hemisphere. Notably, the WM concentration was not apparently reduced.

The GM and WM concentration comparison between patients and healthy controls confirmed the fact that the influence of R-mTLE on the human brain presents a lateralized trend—that is, the atrophy of the GM and WM epileptogenic side of the human brain is more serious than that on the contralateral side. The contralateral side even presents increased WM concentration, which may underpin the lateralized functional connectivity change and support the compensatory mechanism indicated in the article.

ROI Definition for the Entire Brain

Evidence from structural MRI, DTI, and fMRI studies suggested that mTLE is a network disease. A T1-weighted structural MRI–based study constructed whole-brain networks by using the cortical thickness; the network can be used for differentiating patients with mTLE from healthy controls with a accuracy of 93%.[2] A voxel-based DTI study showed that the epileptic networks were principally in the ipsilateral temporal lobe and the limbic system.[3] Graph-theoretical analysis of the cortical thickness network revealed that the small-world networks were disrupted in patients with mTLE.[4] DTI-, structural MRI-, and fMRI-combined studies reported that the cortical atrophy and microstructural white matter impact the resting-state network in mTLE and the altered RSFCs were not confined to hippocampus.[5]

The template for ROI definition can be categorized into anatomic and functional templates. It is difficult to say which kind is more reliable and accurate. In our study, the ROIs used for time-series extraction were defined according to a functional template used in a previous study, which gave an estimation of the underlying functional area architecture.[6] Our study aimed at investigating the R-mTLE from the functional integration perspective; thus, we used the functional template.

The examined ROIs were categorized into 6 RSNs, and we performed analyses from the perspective of functional integration. The ROIs, which facilitated network analysis, were extracted from the previous identified functional networks: 1) the cingulo-opercular network, which includes several regions in the anterior prefrontal cortex, inferior parietal cortex, basal ganglia, dorsal anterior cingulate cortex, insula, thalamus, and cerebellum; 2) the DMN, which includes structures in the hippocampus, posterior cingulate cortex, medial prefrontal cortex, and bilateral inferior parietal cortex; 3) the cerebellum network, which is regarded as a component of the cingulo-opercular network; 4) the visual network, consisting of the primary visual cortex, extra striate visual areas, the lingual gyrus, the fusiform gyrus, and the calcarine gyrus, is involved in visual processing; 5) the sensorimotor network, which includes the primary sensory cortex, primary motor cortex, and supplementary motor cortex; and 6) the frontoparietal network, consisting of the superior parietal cortex and the superior frontal cortex, is involved in attention processing.[6] Although we did not implement the task-related experiment or group-independent component analysis to validate the existing 6 RSNs, many previous studies identified these RSNs by using various method and various subjects.[7-15] Furthermore, these RSNs were believed to represent the functional network.[8,9,15-19] This template includes 160 ROIs. Each ROI was defined as a sphere with a given center coordinate and a radius of 5 mm. The center coordinate for the 160 ROIs is given in the On-line Table.

The center coordinates were defined as the areas of peak activity identified in 5 meta-analyses that focused on error processing, the DMN, memory, language, and sensorimotor functions. Al-

though these functional networks were identified in task-related studies, they were confirmed by many previous resting-state fMRI studies and were further used as RSNs.[15,20-22] Inevitably, using this pre-existing localization of the ROIs can produce bias for the established function of the ROIs; however, it is one of the most important ROI-definition methods.[23]

Selection of the Radius. In our study, the radius of the ROI sphere is 5 mm. However, radii of 4 and 7.5 mm were also tried for time-series extraction. Then the functional connectivity constructed by the time-series according to ROIs with radii of 4 and 7.5 mm was also used for feature selection and classification. The classification results are shown in Fig 1 and On-line Fig 1. When the ROI was defined as a sphere with radii of 4, 5, and 7.5 mm, the corresponding best classification accuracies were 88.1%, 95.2%, and 95.2%. Moreover, when the radius was 5 mm, the accuracy of the classification was more stable. Thus, the ROI defined as a sphere with a radius of 5 mm is reasonable.

Anatomic Template. The automatic anatomic template divided the cerebrum into 90 regions (45 in each hemisphere, but not including the cerebellum and brain stem).[24,25] Here, a previously defined unsampled version of the original automatic anatomic labeling template was adopted for ROI definition, which included 600 ROIs.[26] This template was created via bisecting regions of the automatic anatomic labeling template, and the bisecting boundary was perpendicular to its principal spatial axis to create 2 equally sized subregions. The larger automatic anatomic labeling regions were unsampled more than the smaller automatic anatomic labeling regions to create an atlas of roughly equally sized regions that still obeyed gross anatomic boundaries.

Then, the whole functional connectivity was constructed on the basis of the 600 ROIs. The procedure of feature selection and classification detailed in the main article was then implemented. The highest classification accuracy of 88.1% was obtained. The 221 most discriminative functional connections were then identified and projected to a surface rendering of the mean human cerebrum, which is shown in On-line Fig 3.

The most important finding in On-line Fig 3 is that most of the functional connections contributing to the classification are strengthened. Specifically, the strengthened functional connections were distributed more in the left hemisphere than in the right hemisphere, which was highly consistent with the results in Fig 3.

Feature-Selection Strategy

The imaging neuroscience can be viewed from functional segregation and functional integration perspectives.[27] The structural imaging technique preferred to focus on the functional segregation perspective. However, we paid more attention to the distributed and integrated nature of the R-mTLE. Multivariate pattern analysis was then used to identify groups of the most discriminative functional connections between patients with R-mTLE and healthy controls. Mass univariate methods (eg, 2-sample *t* test) can effectively select the FCs whose strength changed significantly between groups, but they selected the discriminative FCs by looking at only 1 single connection at 1 time and did not consider the interrelationship among FCs, while multivariate pattern analysis views multiple connections as a representation of the difference between the patients and controls.[27,28] Furthermore, groups of FCs identified by multivariate pattern analysis have more generalizability than FCs selected by simple group comparison—that is, the dysfunction in a new patient more likely occurred on the FCs identified by the multivariate pattern analysis.

Cross-Validation and Consensus Functional Connections. Due to our limited number of samples, we used a leave-one-out cross-validation strategy to estimate the generalizability of the classification algorithm. To solve the problem when samples are scarce, M-fold cross-validation uses part of the available samples to learn the model and the rest to test it. We split the data into M roughly equal-sized parts. For the *m*th part, we learned the model for the other M-1 parts of the data and calculated the prediction error of the learned model when testing the *m*th part of the data. We did this for m = 1, 2,…M and rearranged the FCs once for each m. The case M = *n* is known as leave-one-out cross-validation, where *n* is the number of samples.

Because a leave-one-out cross-validation strategy was introduced to estimate the generalization ability of the classifiers (see below) and the training dataset for feature ranking is slightly different in each iteration of the cross-validation, the selected features differed slightly from iteration to iteration. Therefore, the contribution of different regions to classification was not evenly distributed, and some regions formed many highly discriminative FCs with other regions, while some did not. Consensus FCs were introduced here, which were defined as the FCs appearing in at least 1 cross-validation iteration. The discriminative power of the consensus FCs, representing the importance of FCs in identification of the patients with R-mTLE, was denoted by the number of occurrence in all the iterations of the cross-validation. The region weight of the ROI, representing the relative contribution to the identification of patients with R-mTLE, was denoted by accumulating the discriminative power of the consensus FCs related to the ROI.[6]

Univariate Feature Selection. In the main article, a multivariate feature-selection method called "support vector machine recursive feature elimination" was used to identify the most discriminative functional connections. To validate the hemispheric difference of functional connectivity in R-mTLE and compare the multivariate feature-selection method and the traditional mass univariate feature-selection method, we also tried the 2-sample *t* test method for functional connectivity selection. When 17 functional connections were involved, the best classification accuracy of 83.3% was achieved. On the basis of the leave-one-out cross-validation, 73 consensus functional connections were identified and projected to the surface of the human brain as shown in On-line Fig 4.

From On-line Fig 4, we can see that the most discriminative functional connections identified by the univariate feature-selection method (2-sample *t* test) present apparently hemispheric distribution—that is, the functional connections in the right hemisphere were weakened, while those on the left side were strengthened. This result is consistent with the multivariate feature-selection result, which is shown in Fig 3. These 2 results are strong evidence confirming the different R-mTLE-related

changes of functional connectivity in the right and left hemispheres.

Furthermore, the highest classification accuracy achieved by using the functional connections identified by the 2-sample *t* test is 83.3%, which is significantly lower than that obtained by using the functional connections identified by the support vector machine recursive feature elimination. This comparison of the univariate and the multivariate feature-selection methods implied that the multivariate feature selection has an advantage over univariate feature selection. The simple 2-sample *t* test can detect the differences between patients and controls when the sample size is large enough. However, a small sample size will significantly limit its detecting power. The classification accuracy can be viewed as a measure of the generalizability of the feature-selection method. The classification analysis split the samples into training dataset and testing dataset; the feature selection and classifier training were solely implemented on the training dataset; and the testing dataset was completely invisible for the feature selection and classifier training. In this situation, the higher classification accuracy obtained on the testing dataset reflects the selected generalizability of the functional connections—that is, the functional connections give higher classification accuracy reflecting the R-mTLE-related changes in a wider population. From this point of view, the multivariate feature selection has greater potential in dysfunction identification than simple group comparison.

Circle Graph of the Consensus Functional Connections

There were 34 FCs in the right hemisphere; therein 29 FCs were weakened in the patients with R-mTLE and only 5 were strengthened. On the other hand, there were 45 FCs in the left hemisphere, which were all strengthened in patients with R-mTLE rather than in healthy controls. The remaining 45 of the 124 consensus FCs all connected 1 ROI in the left hemisphere and 1 ROI in the right hemisphere, therein 27 FCs were weakened and 18 FCs were strengthened.

Forty of the 124 consensus FCs were categorized as intranetwork FCs; the remaining 84 FCs were categorized as internetwork FCs. Sixteen of the 40 intranetwork FCs were strengthened; 24 were weakened. Fifty-two of the 84 internetwork FCs were strengthened; 32 were weakened. Therefore, more intranetwork FCs were weakened, while more internetwork FCs were strengthened in patients with R-mTLE.

For a better understanding of the inter- and intranetwork distribution of the identified most discriminative functional connections, a circle graph indicating the selected 124 consensus connection distributions and the regional weights of the related ROIs is presented in On-line Fig 5. The region weights of the ROIs related to the identified FCs are displayed in the On-line Table.

The Most Discriminative Functional Connections

Because the first 8 and the first 23 features are important, we added 2 figures depicting the first 8 and first 23 features, respectively. Because the leave-one-out cross-validation strategy was introduced, the first 8 features in each iteration were slightly different. Here, the combination of the first 8 features in each iteration is shown in On-line Fig 5. The number of occurrences for the features was termed "connection strength." The same applies to the first 23 features in On-line Fig 6.

REFERENCES

1. Ashburner J. **A fast diffeomorphic image registration algorithm.** *Neuroimage* 2007;38:95–113
2. Focke NK, Yogarajah M, Symms MR, et al. **Automated MR image classification in temporal lobe epilepsy.** *Neuroimage* 2012;59:356–62
3. Focke NK, Yogarajah M, Bonelli SB, et al. **Voxel-based diffusion tensor imaging in patients with mesial temporal lobe epilepsy and hippocampal sclerosis.** *Neuroimage* 2008;40:728–37
4. Bernhardt BC, Chen Z, He Y, et al. **Graph-theoretical analysis reveals disrupted small-world organization of cortical thickness correlation networks in temporal lobe epilepsy.** *Cereb Cortex* 2011;21:2147–57
5. Voets NL, Beckmann CF, Cole DM, et al. **Structural substrates for resting network disruption in temporal lobe epilepsy.** *Brain* 2012;135:2350–57
6. Dosenbach NU, Nardos B, Cohen AL, et al. **Prediction of individual brain maturity using fMRI.** *Science* 2010;329:1358–61
7. Beckmann CF, DeLuca M, Devlin JT, et al. **Investigations into resting-state connectivity using independent component analysis.** *Philos Trans R Soc Lond B Biol Sci* 2005;360:1001–13
8. Damoiseaux JS, Rombouts SA, Barkhof F, et al. **Consistent resting-state networks across healthy subjects.** *Proc Natl Acad Sci U S A* 2006;103:13848–53
9. De Luca M, Beckmann CF, De Stefano N, et al. **fMRI resting state networks define distinct modes of long-distance interactions in the human brain.** *Neuroimage* 2006;29:1359–67
10. Fransson P. **Spontaneous low-frequency BOLD signal fluctuations: an fMRI investigation of the resting-state default mode of brain function hypothesis.** *Hum Brain Mapp* 2005;26:15–29
11. Salvador R, Suckling J, Coleman MR, et al. **Neurophysiological architecture of functional magnetic resonance images of human brain.** *Cereb Cortex* 2005;15:1332–42
12. van de Ven VG, Formisano E, Prvulovic D, et al. **Functional connectivity as revealed by spatial independent component analysis of fMRI measurements during rest.** *Hum Brain Mapp* 2004;22:165–78
13. van den Heuvel M, Mandl R, Hulshoff Pol H. **Normalized cut group clustering of resting-state FMRI data.** *PLoS One* 2008;3:e2001
14. Power JD, Cohen AL, Nelson SM, et al. **Functional network organization of the human brain.** *Neuron* 2011;72:665–78
15. Repovs G, Csernansky JG, Barch DM. **Brain network connectivity in individuals with schizophrenia and their siblings.** *Biol Psychiatry* 2011;69:967–73
16. Biswal B, Yetkin FZ, Haughton VM, et al. **Functional connectivity in the motor cortex of resting human brain using echo-planar MRI.** *Magn Reson Med* 1995;34:537–41
17. Fox MD, Snyder AZ, Vincent JL, et al. **The human brain is intrinsically organized into dynamic, anticorrelated functional networks.** *Proc Natl Acad Sci U S A* 2005;102:9673–78
18. Cordes D, Haughton VM, Arfanakis K, et al. **Mapping functionally related regions of brain with functional connectivity MR imaging.** *AJNR Am J Neuroradiol* 2000;21:1636–44
19. De Luca M, Smith S, De Stefano N, et al. **Blood oxygenation level dependent contrast resting state networks are relevant to functional activity in the neocortical sensorimotor system.** *Exp Brain Res* 2005;167:587–94
20. Lee MH, Smyser CD, Shimony JS. **Resting-state fMRI: a review of methods and clinical applications.** *AJNR Am J Neuroradiol* 2013;34:1866–72
21. van den Heuvel MP, Hulshoff Pol HE. **Exploring the brain network: a review on resting-state fMRI functional connectivity.** *Eur Neuropsychopharmacol* 2010;20:519–34
22. Tedeschi G, Esposito F. **Neuronal networks observed with resting state functional magnetic resonance imaging in clinical popula-**

tions. In: Bright P. *Neuroimaging Cognitive and Clinical Neuroscience*. North Logan: In Tech; 2012:3
23. Engel J Jr, Thompson PM, Stern JM, et al. **Connectomics and epilepsy.** *Curr Opin Neurol* 2013;26:186–94
24. Tzourio-Mazoyer N, Landeau B, Papathanassiou D, et al. **Automated anatomical labeling of activations in SPM using a macroscopic anatomical parcellation of the MNI MRI single-subject brain.** *Neuroimage* 2002;15:273–89
25. Schmahmann JD, Doyon J, McDonald D, et al. **Three-dimensional MRI atlas of the human cerebellum in proportional stereotaxic space.** *Neuroimage* 1999;10:233–60
26. Hermundstad AM, Bassett DS, Brown KS, et al. **Structural foundations of resting-state and task-based functional connectivity in the human brain.** *Proc Natl Acad Sci U S A* 2013;110:6169–74
27. Friston KJ. **Modalities, modes, and models in functional neuroimaging.** *Science* 2009;326:399–403
28. Haynes JD, Rees G. **Decoding mental states from brain activity in humans.** *Nat Rev Neurosci* 2006;7:976–73

On-line Table: MNI coordinates of the ROIs and the classification weights for the ROIs

Numeric Label	MNI Coordinate			Weight (Normalized)
	X	Y	Z	
1	6	64	3	0.03
2	29	57	18	0
3	−29	57	10	0.02
4	0	51	32	0.28
5	−25	51	27	0.76
6	9	51	16	0
7	−6	50	−1	0.07
8	27	49	26	0.21
9	42	48	−3	0.13
10	−43	47	2	0
11	−11	45	17	0.45
12	39	42	16	0
13	8	42	−5	0.03
14	9	39	20	0.01
15	46	39	−15	0
16	40	36	29	0
17	23	33	47	0
18	34	32	7	0.24
19	−2	30	27	0.04
20	−16	29	54	0.06
21	−1	28	40	0
22	46	28	31	0
23	−52	28	17	0.01
24	−44	27	33	0.83
25	51	23	8	0.10
26	38	21	−1	0
27	9	20	34	0.11
28	−36	18	2	0.07
29	40	17	40	0.0
30	−6	17	34	0.40
31	0	15	45	0.02
32	58	11	14	0.20
33	−46	10	14	0.20
34	44	8	34	0
35	60	8	34	0
36	−42	7	36	0.20
37	−55	7	23	0.13
38	−20	6	7	0
39	14	6	7	0.27
40	−48	6	1	0.45
41	10	5	51	0.02
42	43	1	12	0.01
43	0	−1	52	0.28
44	37	−2	−3	0.06
45	53	−3	32	0.37
46	58	−3	17	0
47	−12	−3	13	0.23
48	−42	−3	11	0
49	−44	−6	49	1
50	−26	−8	54	0.21
51	46	−8	24	0.40
52	−54	−9	23	0
53	44	−11	38	0
54	−47	−12	36	0.35
55	33	−12	16	0
56	−36	−12	15	0
57	−12	−12	6	0.02
58	11	−12	6	0
59	32	−12	2	0.17
60	59	−13	8	0
61	−30	−14	1	0
62	−38	−15	59	0.33
63	52	−15	−13	0.08

Continued on next column

On-line Table: Continued

Numeric Label	MNI Coordinate			Weight (Normalized)
	X	Y	Z	
64	−47	−18	50	0.05
65	46	−20	45	0.05
66	−55	−22	38	0.19
67	−54	−22	22	0.08
68	−54	−22	9	0.04
69	41	−23	55	0
70	42	−24	17	0.08
71	11	−24	2	0
72	−59	−25	−15	0
73	1	−26	31	0.43
74	18	−27	62	0
75	−38	−27	60	0.71
76	−30	−28	9	0
77	−24	−30	64	0.34
78	51	−30	5	0
79	−41	−31	48	0
80	−4	−31	−4	0
81	54	−31	−18	0
82	−41	−37	16	0
83	−53	−37	13	0.02
84	28	−37	−15	0.68
85	−3	−38	45	0
86	34	−39	65	0
87	8	−40	50	0.01
88	−41	−40	42	0
89	58	−41	20	0
90	−8	−41	3	0.16
91	−61	−41	−2	0.04
92	−28	−42	−11	0.08
93	−5	−43	25	0
94	9	−43	25	0
95	43	−43	8	0.35
96	54	−44	43	0.05
97	−55	−44	30	0.01
98	−28	−44	−25	0
99	−35	−46	48	0
100	42	−46	21	0
101	−48	−47	49	0.07
102	−41	−47	29	0
103	−59	−47	11	0.30
104	−53	−50	39	0
105	5	−50	33	0
106	−18	−50	1	0.06
107	44	−52	47	0
108	−5	−52	17	0
109	−24	−54	−21	0
110	−37	−54	−37	0
111	10	−55	17	0.13
112	−6	−56	29	0.02
113	−34	−57	−24	0.19
114	−32	−58	46	0
115	−11	−58	17	0
116	32	−59	41	0.08
117	51	−59	34	0.30
118	−34	−60	−5	0
119	36	−60	−8	0.03
120	−6	−60	−15	0
121	−25	−60	−34	0
122	32	−61	−31	0
123	46	−62	5	0.03
124	−48	−63	35	0
125	−52	−63	15	0.01
126	−44	−63	−7	0

Continued on next page

On-line Table: Continued

Numeric Label	MNI Coordinate			Weight (Normalized)
	X	Y	Z	
127	−16	−64	−21	0.03
128	21	−64	−22	0.19
129	19	−66	−1	0.01
130	1	−66	−24	0.04
131	−34	−67	−29	0
132	11	−68	42	0.01
133	17	−68	20	0.03
134	−36	−69	40	0
135	39	−71	13	0
136	−9	−72	41	0
137	45	−72	29	0
138	−11	−72	−14	0
139	29	−73	29	0.04
140	33	−73	−30	0.33
141	−2	−75	32	0
142	−29	−75	28	0
143	5	−75	−11	0
144	14	−75	−21	0.04
145	−16	−76	33	0
146	−42	−76	26	0.13
147	9	−76	14	0.02
148	15	−77	32	0
149	20	−78	−2	0
150	−21	−79	−33	0.29
151	−6	−79	−33	0
152	−5	−80	9	0
153	29	−81	14	0.34
154	33	−81	−2	0.08
155	18	−81	−33	0.07
156	−37	−83	−2	0
157	−29	−88	8	0.01
158	13	−91	2	0
159	27	−91	2	0
160	−4	−94	12	0

Note:—MNI indicates Montreal Neurological Institute.

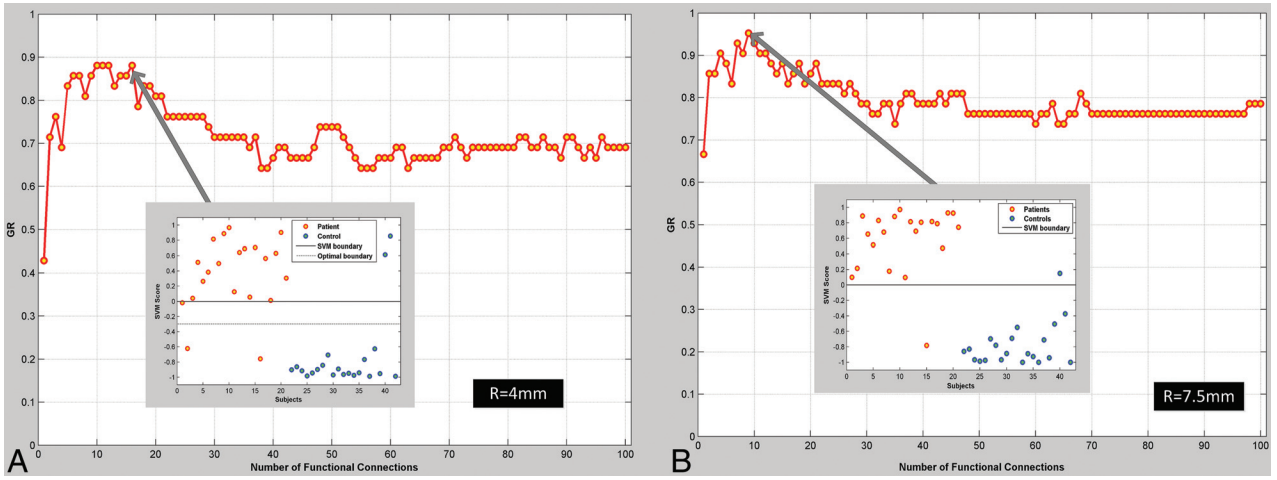

ON-LINE FIG 1. Classification results for patients with R-mTLE and healthy controls by using the ROI with radii of 4 (*A*) and 7.5 mm (*B*). The x-axis indicates the number of connections involved in the classification; the y-axis indicates classification accuracy (as represented by the generalization rate). The subplot illustrates the prediction results of all the subjects with the highest accuracy.

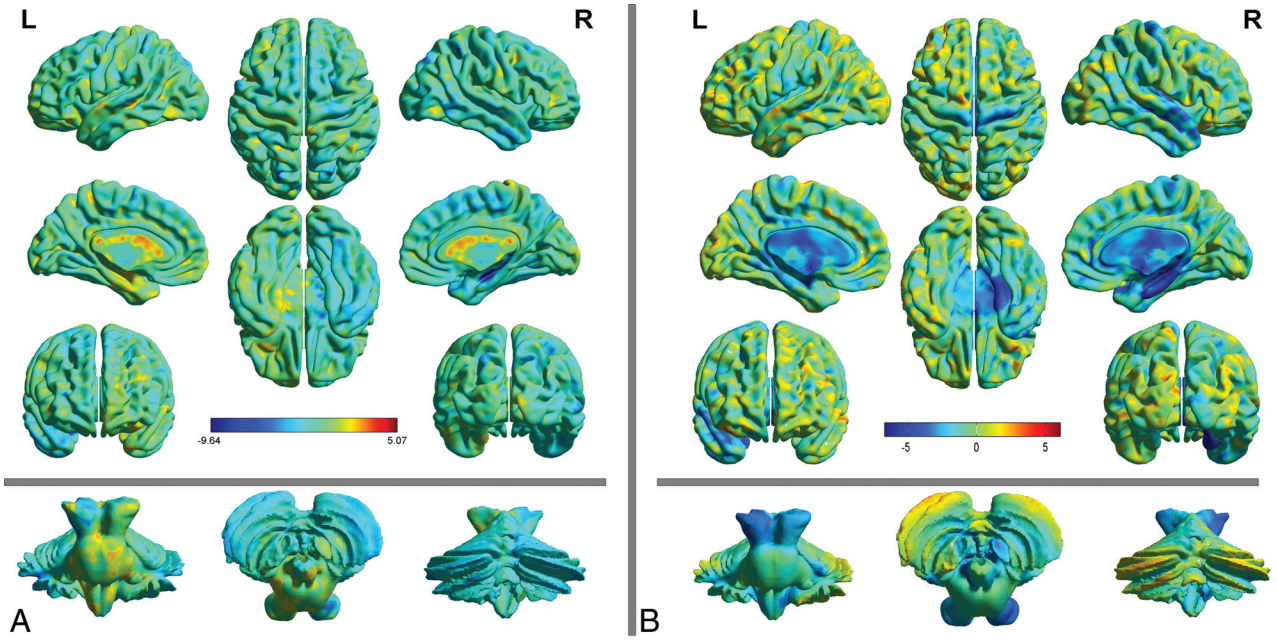

ON-LINE FIG 2. A T-map for group comparison of the GM and WM between the patients with R-mTLE and healthy controls. *A*, The 2-sample *t* test of the GM map for patients with R-mTLE and the healthy controls. *B*, The 2-sample *t* test of the WM map for patients with R-mTLE and the healthy controls. The color bar represents the T-value of the comparison.

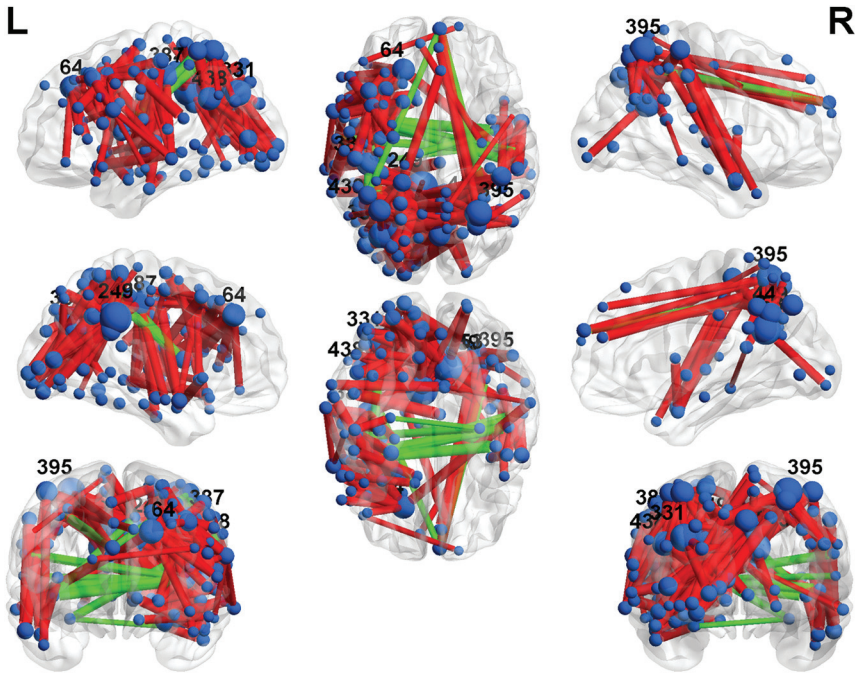

ON-LINE FIG 3. Region weights and connection strengths by using the anatomic template with 600 ROIs. The connections are displayed in a surface rendering of a human brain. The thicknesses of the consensus connections in the leave-one-out cross-validation are scaled by their strengths (which were the normalized occurrences of the first 221 connections during all iterations of the leave-one-out cross-validation). Connections with greater strengths in patients with R-mTLE than in controls are displayed in red, and connections with lower strengths in patients with R-mTLE than in controls are depicted in green. The ROIs related to the selected consensus connections are also scaled by their weights (calculated as the sum of the weights of all connections to and from the ROI of interest) and are displayed. The ROIs are color-coded the same manner as in Figs 3 and 4. The numeric labels for the ROIs in this figure are provided in the On-line Table.

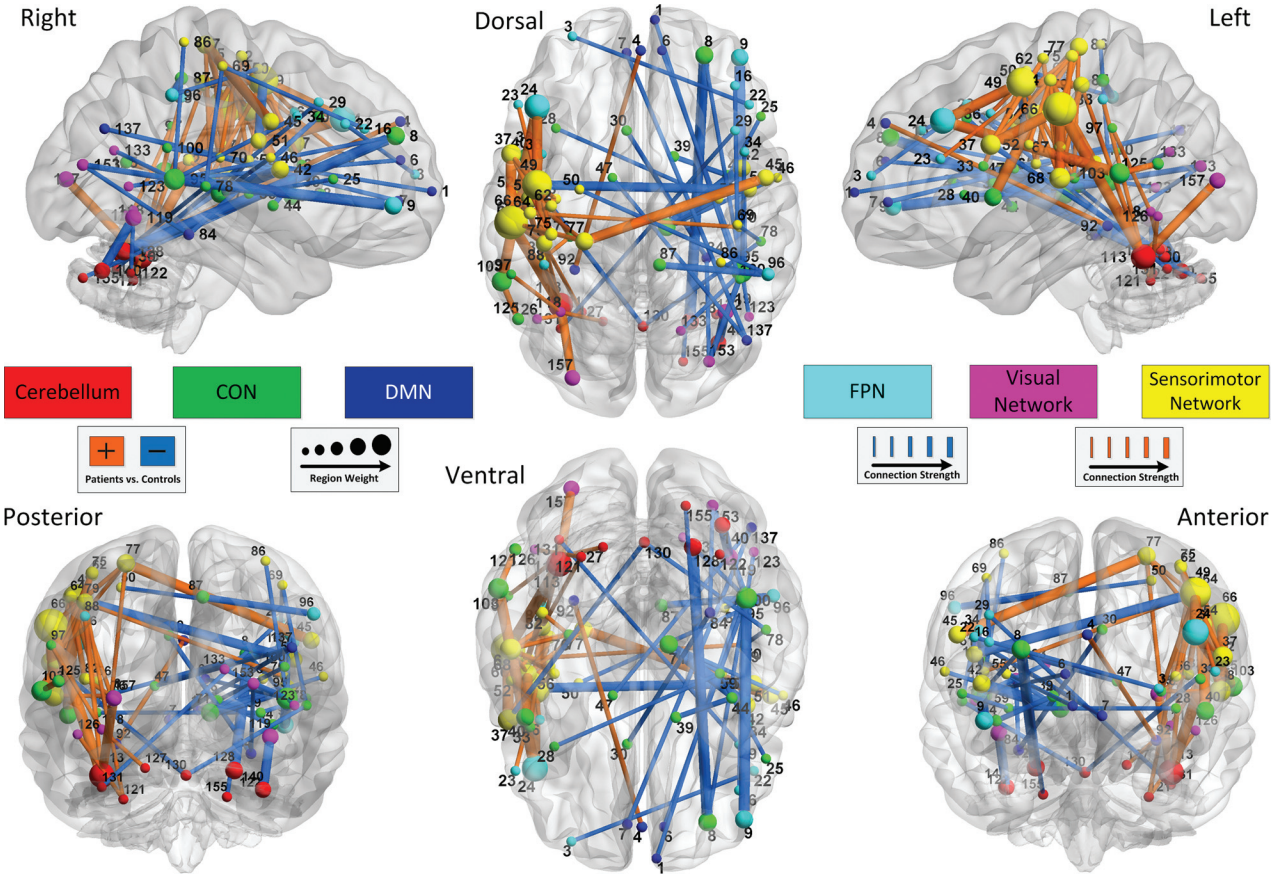

ON-LINE FIG 4. Region weights and connection strengths given by the 2-sample *t* test. The connections are displayed in a surface rendering of a human brain. The thicknesses of the consensus connections in the leave-one-out cross-validation are scaled by their strengths (which were the normalized occurrences of the first 17 connections during all iterations of the leave-one-out cross-validation). Connections with greater strengths in patients with R-mTLE than in controls are displayed in orange; connections with lower strengths in patients with R-mTLE than in controls are depicted in light blue. The ROIs related to the selected consensus connections are also scaled by their weights (calculated as the sum of the weights of all connections to and from the ROI) and are displayed. The ROIs are color-coded in the same manner as in Figs 3 and 4.

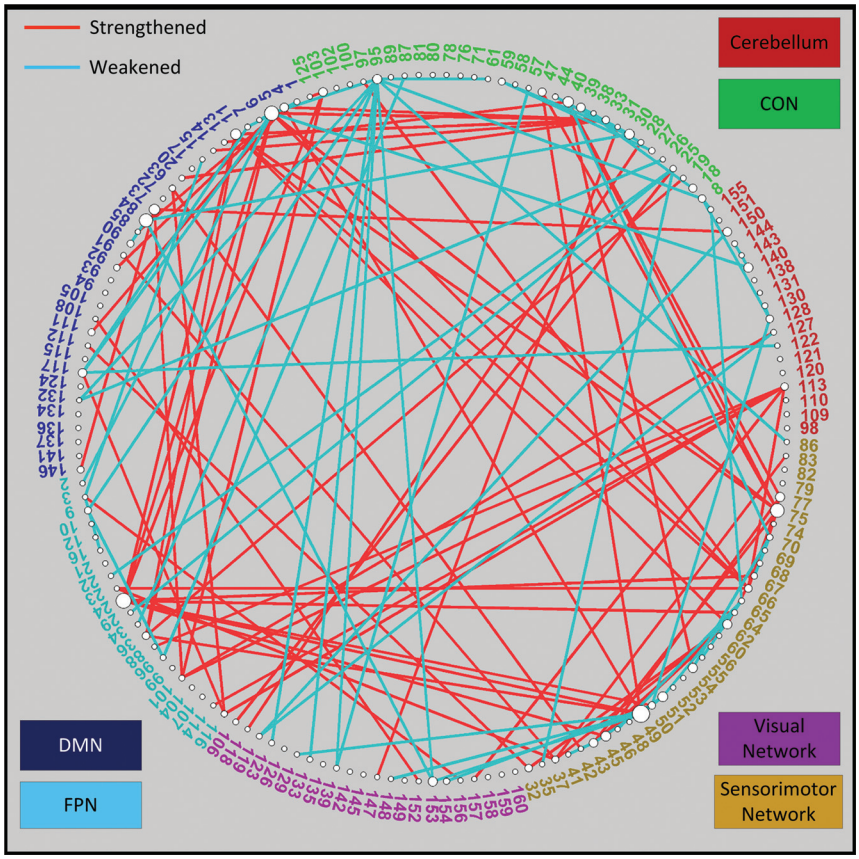

ON-LINE FIG 5. Circle graph indicating the selected consensus connection distribution and the regional weights of related ROIs. The names of the ROIs are color-coded by using the coding scheme in Figs 3 and 4. The cyan lines represent connections that were weakened in patients with R-mTLE, and the red lines represent connections that were strengthened in patients with R-mTLE. The numeric labels for the ROIs in this figure are provided in the On-line Table.

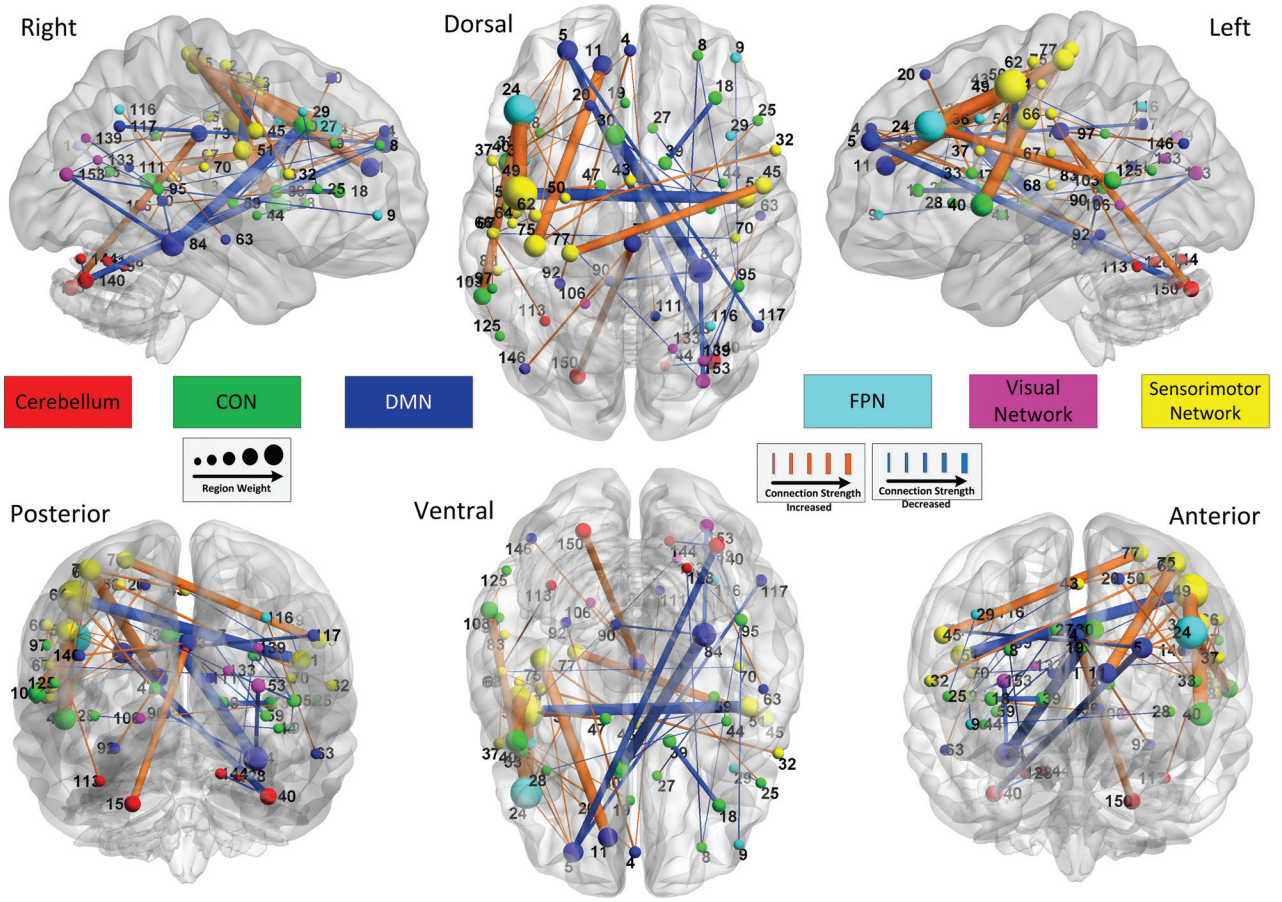

ON-LINE FIG 6. The first 8 most discriminative functional connections. The ROIs are color-coded in the same manner as in Figs 3 and 4.